

## Capacitively and Inductively Coupled Excitons in Bilayer MoS<sub>2</sub>

Lukas Sponfeldner<sup>1,\*</sup>, Nadine Leisgang<sup>1</sup>, Shivangi Shree<sup>2</sup>, Ioannis Paradisanos<sup>2</sup>,  
 Kenji Watanabe<sup>3</sup>, Takashi Taniguchi<sup>4</sup>, Cedric Robert<sup>2</sup>, Delphine Lagarde<sup>2</sup>, Andrea Balocchi<sup>2</sup>,  
 Xavier Marie<sup>2</sup>, Iann C. Gerber<sup>2</sup>, Bernhard Urbaszek<sup>2</sup>, and Richard J. Warburton<sup>1</sup>  
<sup>1</sup>*Department of Physics, University of Basel, Klingelbergstrasse 82, CH-4056 Basel, Switzerland*  
<sup>2</sup>*Université de Toulouse, INSA-CNRS-UPS, LPCNO, 135 Avenue Ranguel, 31077 Toulouse, France*  
<sup>3</sup>*Research Center for Functional Materials, National Institute for Materials Science,  
 1-1 Namiki, Tsukuba 305-0044, Japan*  
<sup>4</sup>*International Center for Materials Nanoarchitectonics, National Institute for Materials Science,  
 1-1 Namiki, Tsukuba 305-0044, Japan*

 (Received 6 August 2021; revised 21 January 2022; accepted 30 June 2022; published 1 September 2022)

The coupling of intralayer A and B excitons and interlayer excitons (IE) is studied in a two-dimensional semiconductor, homobilayer MoS<sub>2</sub>. It is shown that the measured optical susceptibility reveals both the magnitude and the phase of the coupling constants. The IE and B excitons couple via a 0-phase (capacitive) coupling; the IE and A excitons couple via a  $\pi$ -phase (inductive) coupling. The IE-B and IE-A coupling mechanisms are interpreted as hole tunneling and electron-hole exchange, respectively. The couplings imply that even in a monolayer, the A and B excitons have mixed spin states. Using the IE as a sensor, the A-B intravalley exchange coupling is determined. Finally, we realize a bright and highly tunable lowest-energy momentum-direct exciton at high electric fields.

DOI: [10.1103/PhysRevLett.129.107401](https://doi.org/10.1103/PhysRevLett.129.107401)

The elementary excitation at energies close to the band gap of a semiconductor is the exciton, a bound electron-hole pair. The exciton is a prominent feature of the linear optical response of a two-dimensional (2D) semiconductor, for instance monolayer MoS<sub>2</sub>, even at room temperature [1,2]. This is a consequence of the giant exciton binding energies, hundreds of meV [3]. Excitons couple to each other leading to nonlinear optical effects [4,5] and to condensation phenomena, the creation of states with macroscopic quantum correlations [6]. At the few-exciton level, exciton-exciton repulsion in a trap is a potential way to engineer a single-photon emitter [7,8].

Exciton-exciton couplings can arise via the charge of the constituent electrons and holes [9–11]. They can also arise should one of the constituents undergo tunneling. The canonical example is the double quantum well in which moleculelike electronic states form via tunneling between the two quantum wells [12–15]. Recently, moleculelike coupling has been discovered in bilayer 2D semiconductors [16–23].

Here, we probe exciton-exciton couplings in gated-homobilayer MoS<sub>2</sub>. Previous work has revealed an

interlayer exciton (IE) lying energetically between the intralayer A and B excitons [24]. The intralayer excitons are doubly degenerate as an A and a B exist in each monolayer. The IE splits into two lines, IE<sub>1</sub> and IE<sub>2</sub>, on applying a vertical electric field ( $F_z$ ) [25–27], evidence that the IE consists of a hole state delocalized across the two layers bound to an electron localized in one of the layers [24,28]. Avoided crossings were observed as IE<sub>1</sub> and A (IE<sub>2</sub> and B) are brought into resonance [25]. We show here that at very high  $F_z$  the IE<sub>1</sub> becomes the momentum-direct exciton with the lowest energy, that the absorption strengths are sensitive to the phases (signs) of the IE<sub>1</sub>-A, IE<sub>2</sub>-B couplings, and that the IE enables the A-B coupling constant to be determined.

The device is constructed using bilayer MoS<sub>2</sub> [Fig. 1(a)]. The naturally 2H-stacked bilayer MoS<sub>2</sub> is embedded in h-BN; few-layer graphene layers provide a back contact and a top gate; the MoS<sub>2</sub> layer is contacted. Results are presented as a function of  $F_z$  for the smallest possible electron density ( $n$ ). The device is illuminated locally with a weak broadband source. The reflectivity is measured, using the response at large  $n$  as reference, and converted into optical susceptibility using a Kramers-Kronig relationship (see supplement of Ref. [29]). At  $F_z = 0$ , the imaginary part of  $\chi$  (which determines the absorption) shows three peaks: at low energy the intralayer A excitons, at high energy the intralayer B excitons, and in between, the IE [Fig. 2(b)]. These excitonic transitions are shown schematically in Fig. 1(a); the band structure at the  $K$  point is shown in

Published by the American Physical Society under the terms of the [Creative Commons Attribution 4.0 International license](https://creativecommons.org/licenses/by/4.0/). Further distribution of this work must maintain attribution to the author(s) and the published article's title, journal citation, and DOI.

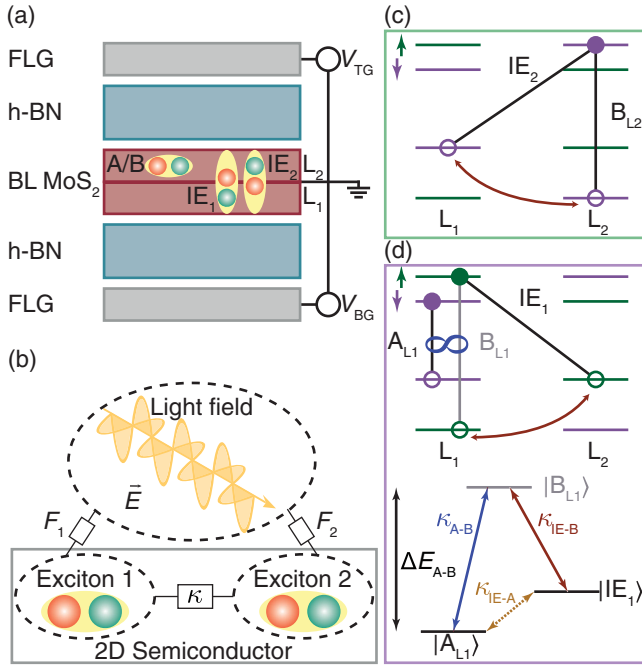


FIG. 1. (a) Schematic of the van der Waals heterostructure consisting of a naturally 2H-stacked homobilayer MoS<sub>2</sub> embedded in h-BN. The MoS<sub>2</sub> bilayer is electrically grounded. The voltages  $V_{TG}$  and  $V_{BG}$  applied to the top and bottom few-layer graphene (FLG) layers create a uniform electric field  $F_z$  across the bilayer. The spatial extents of the intralayer A and B excitons and the interlayer excitons (IE) are sketched. The electrons are depicted in green; the holes in red. MoS<sub>2</sub> bottom (top) layer is denoted as  $L_1$  ( $L_2$ ). (b) Sketch of two coupled excitons in a 2D semiconductor both driven by an external light field. The oscillator strength of each exciton is given by  $F_{1,2}$ ;  $\kappa$  is the coupling constant. (c), (d) Band structure and schematics of excitons in homobilayer MoS<sub>2</sub> at the  $K$  point. (c) Sketch of the microscopic origin of the IE-B coupling mediated by hole tunneling (red arrow). (d) Sketch of the IE-A coupling (top) and a transition diagram (bottom). IE and B are coupled ( $\kappa_{IE-B}$ , red arrow). A and B are coupled through intralayer exchange ( $\kappa_{A-B}$ , blue  $\infty$  symbol). Through the common coupling to B, IE and A are effectively coupled ( $\kappa_{IE-A}$ ).

Figs. 1(c) and 1(d). At high  $F_z$ , there is a clear avoided crossing between IE<sub>2</sub> and B; and a weak avoided crossing between IE<sub>1</sub> and A, as reported in Ref. [25].

At the highest  $F_z$ , IE<sub>1</sub> emerges on the low-energy side of A [Fig. 2(c)]. This means that the ground state exciton is both electric-field tunable and relatively bright. As explained below, we expect the IE<sub>1</sub> to become brighter as it is tuned further below A.

We now focus on the avoided crossings. At the IE-B avoided crossing, one of the B-excitons couples to the IE, the other does not. In Figs. 2(a) and 2(b), we subtract the peak arising from the uncoupled B-exciton (see Supplement [30]). A simple two-level model describes the peak energies convincingly but not the relative intensities. Strikingly, at the  $F_z$  for which the two transitions are

closest together in energy ( $F_{z,0B}$ ), the intensities are quite different: the lower-energy transition is considerably stronger than the higher-energy transition. The IE-A coupling shown in Fig. 2(c) is weaker than the IE-B coupling. One of the A-excitons couples to the IE, the other does not. The absorption from the uncoupled A-exciton is subtracted in Figs. 2(b) and 2(c). The minimum energy separation of the peaks is smaller than the peak broadening. Nevertheless, the avoided crossing has a strong effect on the intensities: as  $F_z$  increases, the IE-like branch enters the avoided crossing with a relatively large intensity, but emerges with a much lower intensity. The IE-A intensity behaviour mimics the behaviour at the IE-B avoided crossing but with one crucial difference. The upper-IE is strong on the low-energy side of the B-exciton; the lower-IE is strong on the high-energy side of the A-exciton.

The optical susceptibility of a quantum well can be calculated from the semiconductor Bloch equations [52–55]. In this approach, the quantum well is treated quantum mechanically. The final result is identical to a completely classical approach in which the quantum well is treated as a 2D array of optical dipoles [56]. Inspired by the success of the purely classical approach, we set up a heuristic description of the IE-B avoided crossing as sketched in Fig. 1(b). The IE and B excitons are treated as optical dipoles, each driven by the same driving field  $\vec{E}$ , but with different oscillator strengths  $F_{1,2}$  [24,57]. A complex linear coupling term  $\kappa = |\kappa|e^{i\phi}$  that carries a phase  $\phi$  is introduced: an IE dipole induces a B dipole, and vice versa. Solving the equations of motion yields an analytic equation for both the eigenenergies  $\hbar\Omega_{\pm}$  and the absorption strengths of the two eigenmodes (see Supplemental Material [30]).

The classical model reproduces both the experimental IE-B peak energies [Fig. 2(a)] and integrated absorption [Fig. 2(d)] extraordinarily well for a good choice of the coupling constant and the ratio of the oscillator strengths. The fits yield an oscillator strength ratio  $F_1/F_2 \approx 5$  and an IE-B coupling strength of  $\kappa = +35.8 \pm 3.6$  meV. The positive sign is inferred from a fitted coupling phase of  $\phi = 0.0 \pm 0.3$ . The IE-A avoided crossing is described with the same model but with the energies appropriate to the lower IE branch and the A exciton along with a different choice of coupling constant. For the A-exciton energy, a quadratic Stark shift is included [58]. Our model reproduces also the IE-A avoided crossing very convincingly. The IE-A coupling is essential to describe the  $F_z$  dependence of the intensities [see Figs. 2(c) and 2(e)]. The fits yield an oscillator strength ratio  $F_1/F_2 \approx 5$  and an IE-A coupling strength of  $\kappa = -3.5 \pm 0.4$  meV. The negative sign is inferred from a fitted coupling phase of  $\phi = \pi \pm 0.3$ . The absorption spectra for the IE-A and IE-B couplings are calculated separately and added together to describe the full  $F_z$  dependence, as shown in Fig. 3.

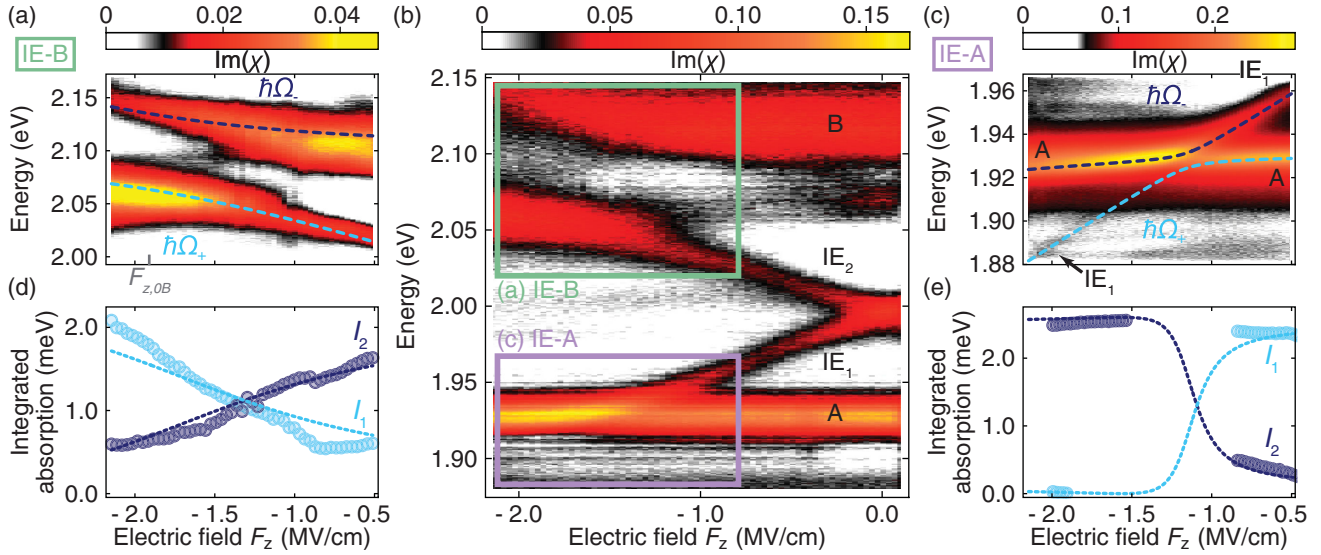


FIG. 2. Absorption ( $\sigma^+$  polarization) of homobilayer MoS<sub>2</sub> as a function of applied electric field  $F_z$ . (b) Absorption over the whole energy range. The green and purple rectangles correspond to the measurement regions centred around the B exciton (a) and the A exciton (c), respectively. The measurements were carried out at  $T = 4.2$  K and magnetic field  $B_z = 9$  T. For clarity, the uncoupled  $B_{L1}$  exciton is removed from (a) and (b), and the uncoupled  $A_{L2}$  exciton is removed from (b) and (c) in a data processing step (see Supplemental Material [30]). In (a),  $F_{z,0B}$  marks the energy crossing for zero coupling. The colored dashed lines in (a) and (c) are fits to the extracted peak energies according to Eqs. S20 and S53 for the eigenenergies  $\hbar\Omega_{\pm}$  (see Supplemental Material [30]). (d) Integrated absorption extracted from the spectra shown in (a). The colored dashed lines are fits to the absorption strength of the eigenmodes  $I_{1,2}$  according to Eq. S33. (e) Integrated absorption extracted from the spectra shown in (c). As the coupling strength is smaller than the line width of the A exciton, only the spectra far from the crossing point can be fitted unambiguously. The colored dashed lines are model fits including the quadratic Stark shift of the A exciton in the initial equations of motion (see Supplemental Material [30]). All parameters extracted from the measured data are summarized in Table I in the Supplemental Material [30].

This model unearths a crucial result: the IE-A coupling constant is of opposite sign to the IE-B coupling constant. The sign of the coupling constant is particularly important

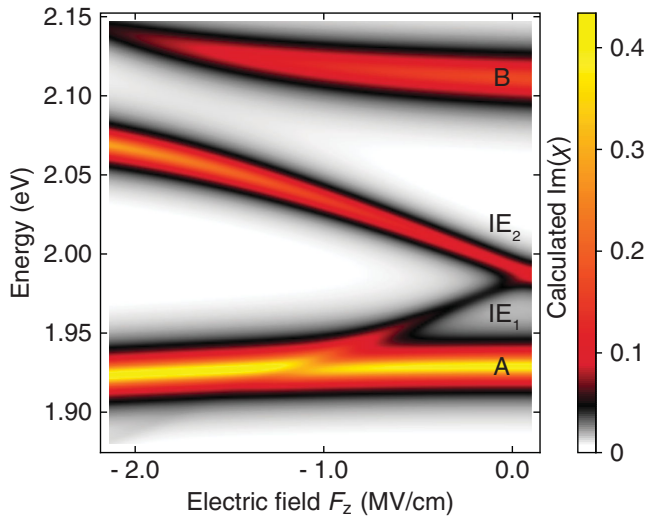


FIG. 3. Color map of the calculated absorption  $\text{Im}(\chi)$  as a function of electric field  $F_z$  with parameters extracted from model fits to the measured data in Fig. 2. The parameters are listed in Table I in the Supplemental Material [30]. Separate models are used to describe the IE-A and IE-B couplings. The  $\text{Im}(\chi)$  is a sum of the two.

in determining the relative strengths of the absorption peaks (see Supplemental Material [30]). We interpret the sign of the coupling by making an analogy to driven, coupled RLC circuits (see Supplemental Material [30]). Two such circuits can be coupled via an impedance. The equations of motion are analogs of those describing the driven optical dipole. The nature of the coupling impedance determines the sign of the coupling constant: coupling via a capacitance (inductance) results in a positive (negative) coupling constant. In this analogy, the IE-B coupling corresponds to a capacitive coupling. This suggests that, at a microscopic level, the IE-B coupling involves the movement of charge—it is consistent with hole tunneling from one layer to the other [24]. Conversely, the IE-A coupling corresponds to an inductive coupling. This points to a completely different coupling mechanism, as discussed below.

The model provides an explanation for the  $F_z$  dependent absorption strengths in Figs. 2(b) and 3. We take the IE-A coupling as an example. Without a coupling, both IE and A respond directly to the driving field. A has the stronger response: the induced dipole moment is in phase with the drive for energies well below the bare A energy and out of phase for energies well above the bare A energy (the standard behavior for a driven harmonic oscillator). With a coupling, each eigenmode is a dressed state of IE and A. At detunings far from the avoided crossing, there is an A-like

and an IE-like eigenmode. The IE-like mode is driven by two sources: the field acting directly on the IE, and via its coupling to A. Now the sign of the coupling plays a crucial role. If the coupling has a negative sign, then for energies above (below) the bare A energy, these two terms have the same (opposite) sign and interfere constructively (destructively). At a particular detuning, the destructive interference is complete and the absorption of one mode disappears. Even at energies far from the avoided crossing, this interference has a strong effect on the IE absorption. The picture inverts for a positive coupling, the IE-B coupling. In this case, the IE-like mode is boosted (suppressed) when it lies below (above) the bare B energy. At  $F_z = 0$ , the IE is far from the avoided crossing with both A and B excitons but its absorption strength is boosted by its coupling to both A and B. In simple terms, the dielectric constant at the IE resonance is strongly influenced by the strong A and B resonances.

We look for a microscopic explanation for the different IE-A and IE-B couplings. To do this, we describe the band structure of bilayer MoS<sub>2</sub> at the GW level (one-particle Green's function  $G$ , dynamically screened Coulomb

interaction  $W$ ), and use these states to construct excitons by solving the Bethe-Salpeter equation (BSE) (see Fig. 4 and Supplemental Material [30]). The results describe the general behavior of the experiments very well as revealed by a comparison of the calculated relative absorption strengths in Figs. 4(b) and 4(c) with the measured integrated absorption in Fig. 2(e). (Exact quantitative agreement is not expected as the model assumes that the MoS<sub>2</sub> bilayers are located in vacuum—it does not take into account the full dielectric environment.) As in the experiment, the IE are relatively strong when they lie energetically between the bare A and the bare B resonances but weaker when they lie out of this energy window [Figs. 4(b) and 4(c)]. The GW + BSE results can be parametrized by the coupled-dipole model (see Supplemental Material [30]).

An analysis of the spin and orbital composition of the excitons provides an explanation for both the IE-B and IE-A couplings. The IE-B coupling arises via hole tunneling [see Fig. 1(c)]. The large IE-B coupling constant, +35.8 meV, reflects the efficient hole tunneling. Conversely, the IE-A coupling arises via a weak admixture between the A and B excitons in the same valley and layer, as shown schematically in Fig. 1(d). This exciton admixture was proposed in Ref. [59] for MoS<sub>2</sub> monolayers and is found also in our bilayer calculations (Fig. 4). This means that both IE and A couple to B. IE and A then acquire an effective coupling, a second-order effect.

In this analysis, depicted in Fig. 1(d), the IE-A coupling is determined by  $\kappa_{\text{IE-A}} = -(\kappa_{\text{A-B}}\kappa_{\text{IE-B}}/\Delta E_{\text{A-B}})$  (with the sign convention employed here) where  $\kappa_{\text{IE-B}}$  is the IE-B coupling,  $\kappa_{\text{A-B}}$  the A-B coupling, and  $\Delta E_{\text{A-B}}$  is the energy splitting between A and B [60]. The experiment measures  $\kappa_{\text{IE-A}} = -3.5$  meV,  $\kappa_{\text{IE-B}} = 35.8$  meV, and  $\Delta E_{\text{A-B}} = -170$  meV. In turn, this determines  $\kappa_{\text{A-B}}$ . We find  $\kappa_{\text{A-B}} = -16.6 \pm 2.5$  meV. In other words, by using the IE as a tunable probe, we are able to determine the A-B coupling energy. This is an important quantity—it arises even in a MoS<sub>2</sub> monolayer and determines to what extent spin is a good quantum number in the fundamental exciton [59,61].

We state four main conclusions. First, a 2D semiconductor system, homobilayer MoS<sub>2</sub>, is discovered for which the lowest-energy momentum-direct exciton is both electric-field tunable and bright, gaining in absorption strength as the field is increased. This is not the case for a monolayer (bright but without field tunability) or a heterobilayer (field-tunable but dim). This is potentially useful in transporting and trapping excitons with locally varying electric fields. Second, in homobilayer MoS<sub>2</sub>, the IE and B excitons couple via hole tunneling; the IE and A excitons couple via an exchange-induced A-B admixture. This difference results in coupling constants of opposite sign (IE-B coupling phase 0, IE-A coupling phase  $\pi$ ). Hybridized intra- and interlayer excitons can be tuned into a regime where one eigenmode is as bright as the intralayer

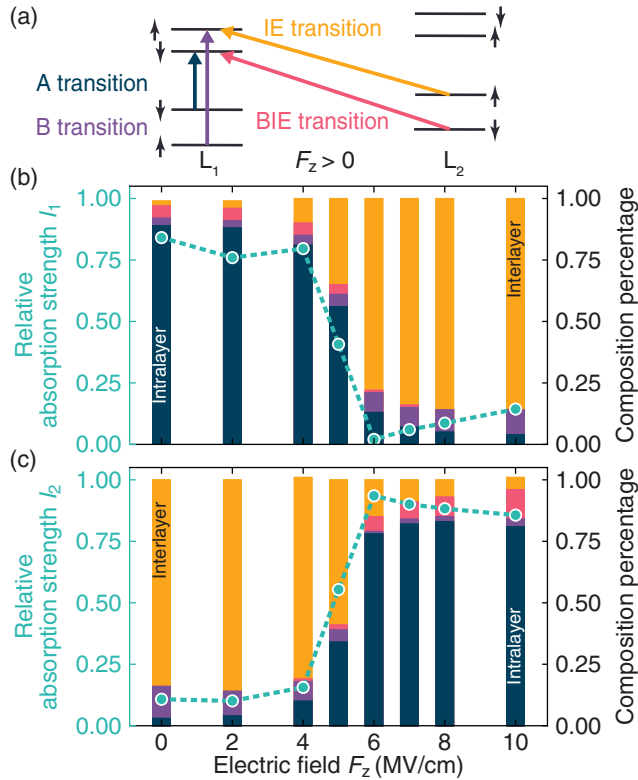


FIG. 4. (a) Main excitonic transitions contributing to the IE-A dressed state. BIE denotes the higher-energy interlayer transition. (b),(c) Relative absorption strength of eigenmode-1  $I_1$  (b) and eigenmode-2  $I_2$  (c) of the IE-A coupling as a function of electric field determined by GW + BSE calculations. The cyan dashed line is a guide to the eye. The colored bars indicate the composition percentage; the colors match those used in (a).

component yet retains the electric dipole moment of the interlayer component. This combination of properties is very useful for creating exciton- or polaron-polaritons with highly nonlinear optical properties [62,63]. Third, we determine the A-B coupling, a result which is also relevant for a monolayer. By using IE as a sensor, we can measure the A-B coupling precisely—experiments on a monolayer are much harder to interpret. We find an A-B coupling of  $-16.6$  meV. Equivalently, the A-like eigenstate is  $|A\rangle + \epsilon|B\rangle$  with  $|\epsilon| \simeq 10\%$ , and vice versa for the B-like eigenstate. The A-B coupling implies that spin is an imperfect quantum number for the A and B excitons in the same valley. This is a basic property of MoS<sub>2</sub>. Finally, we show that a measurement of the optical susceptibility enables not just the magnitude but also the phase of the exciton-exciton couplings to be determined (see Fig. 3). The coupling model can be readily applied to other transition metal dichalcogenides bilayer systems where band hybridization leads to mixed excitonic states [16,19,22,23,64,65].

We point out that the driven coupled-oscillator model has a general validity—it is by no means limited to excitons in the optical domain. We note for instance that it describes the response of two coupled gatemons at microwave frequencies where a clear destructive interference is observed in the lower-frequency branch [66]. The model shows how a weak resonance can be made visible by bringing it into near degeneracy with a strong resonance. All that is required is a coupling between the two resonances. Furthermore, in the case of a weak coupling, although the energies are only slightly perturbed, the absorption strengths are strongly modified by the coupling. This sensitivity is very useful in cases where the couplings are potentially weak or completely unknown. Examples include hybrid systems—for instance, an exciton or a spin coupled to a mechanical mode.

We thank Christoph Bruder for fruitful discussions and Jonas Roch for expert experimental assistance. Basel acknowledges funding from the Swiss Nanoscience Institute (SNI), Ph.D. School Quantum Computing and Quantum Technology (QCQT), SNF (Project No. 200020\_175748), and NCCR QSIT. Toulouse acknowledges funding from ANR MagicValley, ANR IXTASE, ANR HiLight, ITN 4PHOTON Marie Skłodowska Curie Grant Agreement No. 721394 and the Institut Universitaire de France. K. W. and T. T. acknowledge support from the Elemental Strategy Initiative conducted by the MEXT, Japan (Grant No. JPMXP0112101001) and JSPS KAKENHI (Grants No. 19H05790 and No. JP20H00354). I. C. G. thanks the CALMIP initiative for the generous allocation of computational time, through Project No. p0812, as well as GENCI-CINES and GENCI-IDRIS, Grant No. A010096649.

\*Corresponding author.

lukas.sponfeldner@unibas.ch

- [1] K. F. Mak, C. Lee, J. Hone, J. Shan, and T. F. Heinz, Atomically Thin MoS<sub>2</sub>: A New Direct-Gap Semiconductor, *Phys. Rev. Lett.* **105**, 136805 (2010).
- [2] A. Splendiani, L. Sun, Y. Zhang, T. Li, J. Kim, C.-Y. Chim, G. Galli, and F. Wang, Emerging photoluminescence in monolayer MoS<sub>2</sub>, *Nano Lett.* **10**, 1271 (2010).
- [3] A. Chernikov, T. C. Berkelbach, H. M. Hill, A. Rigosi, Y. Li, O. B. Aslan, D. R. Reichman, M. S. Hybertsen, and T. F. Heinz, Exciton Binding Energy and Nonhydrogenic Rydberg Series in Monolayer WS<sub>2</sub>, *Phys. Rev. Lett.* **113**, 076802 (2014).
- [4] G. Wang, X. Marie, I. Gerber, T. Amand, D. Lagarde, L. Bouet, M. Vidal, A. Balocchi, and B. Urbaszek, Giant Enhancement of the Optical Second-Harmonic Emission of WSe<sub>2</sub> Monolayers by Laser Excitation at Exciton Resonances, *Phys. Rev. Lett.* **114**, 097403 (2015).
- [5] T. Jakubczyk, V. Delmonte, M. Koperski, K. Nogajewski, C. Faugeras, W. Langbein, M. Potemski, and J. Kasprzak, Radiatively limited dephasing and exciton dynamics in MoS<sub>2</sub> monolayers revealed with four-wave mixing microscopy, *Nano Lett.* **16**, 5333 (2016).
- [6] J. Kasprzak, M. Richard, S. Kundermann, A. Baas, P. Jeambrun, J. M. J. Keeling, F. M. Marchetti, M. H. Szymańska, R. André, J. L. Staehli, V. Savona, P. B. Littlewood, B. Deveaud, and L. S. Dang, Bose-Einstein condensation of exciton polaritons, *Nature (London)* **443**, 409 (2006).
- [7] A. Delteil, T. Fink, A. Schade, S. Höfling, C. Schneider, and A. İmamoğlu, Towards polariton blockade of confined exciton-polaritons, *Nat. Mater.* **18**, 219 (2019).
- [8] G. Muñoz-Matutano, A. Wood, M. Johnsson, X. Vidal, B. Q. Baragiola, A. Reinhard, A. Lemaître, J. Bloch, A. Amo, G. Nogues, B. Besga, M. Richard, and T. Volz, Emergence of quantum correlations from interacting fibre-cavity polaritons, *Nat. Mater.* **18**, 213 (2019).
- [9] C. Ciuti, V. Savona, C. Piermarocchi, A. Quattropani, and P. Schwendimann, Role of the exchange of carriers in elastic exciton-exciton scattering in quantum wells, *Phys. Rev. B* **58**, 7926 (1998).
- [10] V. Shahnazaryan, I. Iorsh, I. A. Shelykh, and O. Kyriienko, Exciton-exciton interaction in transition-metal dichalcogenide monolayers, *Phys. Rev. B* **96**, 115409 (2017).
- [11] D. Erkensten, S. Brem, and E. Malic, Exciton-exciton interaction in transition metal dichalcogenide monolayers and van der Waals heterostructures, *Phys. Rev. B* **103**, 045426 (2021).
- [12] R. Ferreira, C. Delalande, H. W. Liu, G. Bastard, B. Etienne, and J. F. Palmier, Resonances in the excitonic transfer in biased double quantum wells, *Phys. Rev. B* **42**, 9170 (1990).
- [13] A. M. Fox, D. A. B. Miller, G. Livescu, J. E. Cunningham, and W. Y. Jan, Excitonic effects in coupled quantum wells, *Phys. Rev. B* **44**, 6231 (1991).
- [14] K. Sivalertporn, L. Mouchliadis, A. L. Ivanov, R. Philp, and E. A. Muljarov, Direct and indirect excitons in semiconductor coupled quantum wells in an applied electric field, *Phys. Rev. B* **85**, 045207 (2012).

- [15] P. Andreakou, S. Cronenberger, D. Scalbert, A. Nalitov, N. A. Gippius, A. V. Kavokin, M. Nawrocki, J. R. Leonard, L. V. Butov, K. L. Campman, A. C. Gossard, and M. Vladimirova, Nonlinear optical spectroscopy of indirect excitons in coupled quantum wells, *Phys. Rev. B* **91**, 125437 (2015).
- [16] E. M. Alexeev, D. A. Ruiz-Tijerina, M. Danovich, M. J. Hamer, D. J. Terry, P. K. Nayak, S. Ahn, S. Pak, J. Lee, J. I. Sohn, M. R. Molas, M. Koperski, K. Watanabe, T. Taniguchi, K. S. Novoselov, R. V. Gorbachev, H. S. Shin, V. I. Fal'ko, and A. I. Tartakovskii, Resonantly hybridized excitons in moiré superlattices in van der Waals heterostructures, *Nature (London)* **567**, 81 (2019).
- [17] W.-T. Hsu, B.-H. Lin, L.-S. Lu, M.-H. Lee, M.-W. Chu, L.-J. Li, W. Yao, W.-H. Chang, and C.-K. Shih, Waals bilayers through stacking configuration, band alignment, and valley spin, *Sci. Adv.* **5**, eaax7407 (2019).
- [18] Y. Shimazaki, I. Schwartz, K. Watanabe, T. Taniguchi, M. Kroner, and A. İmamoğlu, Strongly correlated electrons and hybrid excitons in a moiré heterostructure, *Nature (London)* **580**, 472 (2020).
- [19] J. Sung, Y. Zhou, G. Scuri, V. Zólyomi, T. I. Andersen, H. Yoo, D. S. Wild, A. Y. Joe, R. J. Gelly, H. Heo, S. J. Magorrian, D. Bérubé, A. M. M. Valdivia, T. Taniguchi, K. Watanabe, M. D. Lukin, P. Kim, V. I. Fal'ko, and H. Park, Broken mirror symmetry in excitonic response of reconstructed domains in twisted MoS<sub>2</sub>/MoS<sub>2</sub> bilayers, *Nat. Nanotechnol.* **15**, 750 (2020).
- [20] P. Merkl, F. Mooshammer, S. Brem, A. Girmhuber, K.-Q. Lin, L. Weigl, M. Liebich, C.-K. Yong, R. Gillen, J. Maultzsch, J. M. Lupton, E. Malic, and R. Huber, Twist-tailoring Coulomb correlations in van der Waals homobilayers, *Nat. Commun.* **11**, 2167 (2020).
- [21] L. Zhang, Z. Zhang, F. Wu, D. Wang, R. Gogna, S. Hou, K. Watanabe, T. Taniguchi, K. Kulkarni, T. Kuo, S. R. Forrest, and H. Deng, Twist-angle dependence of moiré excitons in WS<sub>2</sub>/MoSe<sub>2</sub> heterobilayers, *Nat. Commun.* **11**, 5888 (2020).
- [22] Y. Tang, J. Gu, S. Liu, K. Watanabe, T. Taniguchi, J. Hone, K. F. Mak, and J. Shan, Tuning layer-hybridized moiré excitons by the quantum-confined Stark effect, *Nat. Nanotechnol.* **16**, 52 (2021).
- [23] L. P. McDonnell, J. J. S. Viner, D. A. Ruiz-Tijerina, P. Rivera, X. Xu, V. I. Fal'ko, and D. C. Smith, Superposition of intra- and inter-layer excitons in twistrionic MoSe<sub>2</sub>/WSe<sub>2</sub> bilayers probed by resonant Raman scattering, *2D Mater.* **8**, 035009 (2021).
- [24] I. C. Gerber, E. Courtade, S. Shree, C. Robert, T. Taniguchi, K. Watanabe, A. Balocchi, P. Renucci, D. Lagarde, X. Marie, and B. Urbaszek, Interlayer excitons in bilayer MoS<sub>2</sub> with strong oscillator strength up to room temperature, *Phys. Rev. B* **99**, 035443 (2019).
- [25] N. Leisgang, S. Shree, I. Paradisanos, L. Sponfeldner, C. Robert, D. Lagarde, A. Balocchi, K. Watanabe, T. Taniguchi, X. Marie, R. J. Warburton, I. C. Gerber, and B. Urbaszek, Giant Stark splitting of an exciton in bilayer MoS<sub>2</sub>, *Nat. Nanotechnol.* **15**, 901 (2020).
- [26] E. Lorchat, M. Selig, F. Katsch, K. Yumigeta, S. Tongay, A. Knorr, C. Schneider, and S. Höfling, Excitons in Bilayer MoS<sub>2</sub> Displaying a Colossal Electric Field Splitting and Tunable Magnetic Response, *Phys. Rev. Lett.* **126**, 037401 (2021).
- [27] N. Peimyoo, T. Deilmann, F. Withers, J. Escobar, D. Nutting, T. Taniguchi, K. Watanabe, A. Taghizadeh, M. F. Craciun, K. S. Thygesen, and S. Russo, Electrical tuning of optically active interlayer excitons in bilayer MoS<sub>2</sub>, *Nat. Nanotechnol.* **16**, 888 (2021).
- [28] R. Pisoni, T. Davatz, K. Watanabe, T. Taniguchi, T. Ihn, and K. Ensslin, Absence of Interlayer Tunnel Coupling of K-Valley Electrons in Bilayer MoS<sub>2</sub>, *Phys. Rev. Lett.* **123**, 117702 (2019).
- [29] J. G. Roch, G. Froehlicher, N. Leisgang, P. Makk, K. Watanabe, T. Taniguchi, and R. J. Warburton, Spin-polarized electrons in monolayer MoS<sub>2</sub>, *Nat. Nanotechnol.* **14**, 432 (2019).
- [30] See Supplemental Material at <http://link.aps.org/supplemental/10.1103/PhysRevLett.129.107401> for additional information on the exciton-exciton coupling model, the sample fabrication, the experimental methods, and details on the GW + BSE calculations, which includes Refs. [31–51].
- [31] P. J. Zomer, M. H. D. Guimarães, J. C. Brant, N. Tombros, and B. J. van Wees, Fast pick up technique for high quality heterostructures of bilayer graphene and hexagonal boron nitride, *Appl. Phys. Lett.* **105**, 013101 (2014).
- [32] T. Taniguchi and K. Watanabe, Synthesis of high-purity boron nitride single crystals under high pressure by using Ba–BN solvent, *J. Cryst. Growth* **303**, 525 (2007).
- [33] A. Laturia, M. L. V. d. Put, and W. G. Vandenberghe, Dielectric properties of hexagonal boron nitride and transition metal dichalcogenides: From monolayer to bulk, *npj 2D Mater. Appl.* **2**, 6 (2018).
- [34] P. Back, M. Sidler, O. Cotlet, A. Srivastava, N. Takemura, M. Kroner, and A. İmamoğlu, Giant Paramagnetism-Induced Valley Polarization of Electrons in Charge-Tunable Monolayer MoSe<sub>2</sub>, *Phys. Rev. Lett.* **118**, 237404 (2017).
- [35] M. Frimmer and L. Novotny, The classical Bloch equations, *Am. J. Phys.* **82**, 947 (2014).
- [36] M. Kira and S. W. Koch, Many-body correlations and excitonic effects in semiconductor spectroscopy, *Prog. Quantum Electron.* **30**, 155 (2006).
- [37] C. Cohen-Tannoudji, B. Diu, and F. Laloë, *Quantum Mechanics*, Vol. 2 (Wiley, New York, 2005).
- [38] J. G. Roch, N. Leisgang, G. Froehlicher, P. Makk, K. Watanabe, T. Taniguchi, C. Schönenberger, and R. J. Warburton, Quantum-confined stark effect in a MoS<sub>2</sub> monolayer van der Waals heterostructure, *Nano Lett.* **18**, 1070 (2018).
- [39] T. G. Pedersen, Exciton Stark shift and electroabsorption in monolayer transition-metal dichalcogenides, *Phys. Rev. B* **94**, 125424 (2016).
- [40] G. Kresse and J. Hafner, *Ab initio* molecular dynamics for liquid metals, *Phys. Rev. B* **47**, 558 (1993).
- [41] G. Kresse and J. Furthmüller, Efficient iterative schemes for *ab initio* total-energy calculations using a plane-wave basis set, *Phys. Rev. B* **54**, 11169 (1996).
- [42] P. E. Blöchl, Projector augmented-wave method, *Phys. Rev. B* **50**, 17953 (1994).

- [43] G. Kresse and D. Joubert, From ultrasoft pseudopotentials to the projector augmented-wave method, *Phys. Rev. B* **59**, 1758 (1999).
- [44] S. Grimme, J. Antony, S. Ehrlich, and H. Krieg, A consistent and accurate ab initio parametrization of density functional dispersion correction (DFT-D) for the 94 elements H-Pu, *J. Chem. Phys.* **132**, 154104 (2010).
- [45] J. Heyd and G. E. Scuseria, Assessment and validation of a screened Coulomb hybrid density functional, *J. Chem. Phys.* **120**, 7274 (2004).
- [46] J. Heyd, J. E. Peralta, G. E. Scuseria, and R. L. Martin, Energy band gaps and lattice parameters evaluated with the Heyd-Scuseria-Ernzerhof screened hybrid functional, *J. Chem. Phys.* **123**, 174101 (2005).
- [47] J. Paier, M. Marsman, K. Hummer, G. Kresse, I. C. Gerber, and J. G. Ángyán, Screened hybrid density functionals applied to solids, *J. Chem. Phys.* **124**, 154709 (2006).
- [48] M. Shishkin and G. Kresse, Implementation and performance of the frequency-dependent GW method within the PAW framework, *Phys. Rev. B* **74**, 035101 (2006).
- [49] A. A. Mostofi, J. R. Yates, Y.-S. Lee, I. Souza, D. Vanderbilt, and N. Marzari, wannier90: A tool for obtaining maximally-localised Wannier functions, *Comput. Phys. Commun.* **178**, 685 (2008).
- [50] W. Hanke and L. J. Sham, Many-Particle Effects in the Optical Excitations of a Semiconductor, *Phys. Rev. Lett.* **43**, 387 (1979).
- [51] M. Rohlfing and S. G. Louie, Electron-Hole Excitations in Semiconductors and Insulators, *Phys. Rev. Lett.* **81**, 2312 (1998).
- [52] M. Lindberg and S. W. Koch, Effective Bloch equations for semiconductors, *Phys. Rev. B* **38**, 3342 (1988).
- [53] S. W. Koch, M. Kira, G. Khitrova, and H. M. Gibbs, Semiconductor excitons in new light, *Nat. Mater.* **5**, 523 (2006).
- [54] H. Haug and S. W. Koch, *Quantum Theory of the Optical and Electronic Properties of Semiconductors* (World Scientific, Singapore, 2009).
- [55] C. F. Klingshirm, *Semiconductor Optics* (Springer, Berlin, Heidelberg, 2012).
- [56] K. Karrai and R. J. Warburton, Optical transmission and reflection spectroscopy of single quantum dots, *Superlattices Microstruct.* **33**, 311 (2003).
- [57] T. Deilmann and K. S. Thygesen, Interlayer Excitons with Large Optical Amplitudes in Layered van der Waals Materials, *Nano Lett.* **18**, 2984 (2018).
- [58] D. A. B. Miller, D. S. Chemla, T. C. Damen, A. C. Gossard, W. Wiegmann, T. H. Wood, and C. A. Burrus, Band-Edge Electroabsorption in Quantum Well Structures: The Quantum-Confinement Stark Effect, *Phys. Rev. Lett.* **53**, 2173 (1984).
- [59] L. Guo, M. Wu, T. Cao, D. M. Monahan, Y.-H. Lee, S. G. Louie, and G. R. Fleming, Exchange-driven intravalley mixing of excitons in monolayer transition metal dichalcogenides, *Nat. Phys.* **15**, 228 (2019).
- [60] P. Löwdin, A note on the quantum-mechanical perturbation theory, *J. Chem. Phys.* **19**, 1396 (1951).
- [61] Y. Wang, Z. Wang, W. Yao, G.-B. Liu, and H. Yu, Interlayer coupling in commensurate and incommensurate bilayer structures of transition-metal dichalcogenides, *Phys. Rev. B* **95**, 115429 (2017).
- [62] L. B. Tan, O. Cotlet, A. Bergschneider, R. Schmidt, P. Back, Y. Shimazaki, M. Kroner, and A. İmamoğlu, Interacting Polaron-Polaritons, *Phys. Rev. X* **10**, 021011 (2020).
- [63] C. Louca, A. Genco, S. Chiavazzo, T. P. Lyons, S. Randerson, C. Trovatiello, P. Claronino, R. Jayaprakash, K. Watanabe, T. Taniguchi, S. D. Conte, D. G. Lidzey, G. Cerullo, O. Kyriienko, and A. I. Tartakovskii, Nonlinear interactions of dipolar excitons and polaritons in MoS<sub>2</sub> bilayers, [arXiv:2204.00485](https://arxiv.org/abs/2204.00485).
- [64] D. A. Ruiz-Tijerina and V. I. Fal'ko, Interlayer hybridization and moiré superlattice minibands for electrons and excitons in heterobilayers of transition-metal dichalcogenides, *Phys. Rev. B* **99**, 125424 (2019).
- [65] J. Kiemle, F. Sigger, M. Lorke, B. Miller, K. Watanabe, T. Taniguchi, A. Holleitner, and U. Wurstbauer, Control of the orbital character of indirect excitons in MoS<sub>2</sub>/WS<sub>2</sub> heterobilayers, *Phys. Rev. B* **101**, 121404(R) (2020).
- [66] L. Casparis, T. W. Larsen, M. S. Olsen, F. Kuemmeth, P. Krogstrup, J. Nygård, K. Petersson, and C. M. Marcus, Gatemon Benchmarking and Two-Qubit Operations, *Phys. Rev. Lett.* **116**, 150505 (2016).